Electronic structure of thiol-bonded self-assembled monolayers: Impact of coverage

Lorenz Romaner,[1] Georg Heimel,[2,3] and Egbert Zojer[1]
[1]*Institute of Solid State Physics, Graz University of Technology, Petersgasse 16, A-8010 Graz, Austria*
[2]*School of Chemistry and Biochemistry and Center for Organic Photonics and Electronics, Georgia Institute of Technology, Atlanta, Georgia 30332-0400, USA*
[3]*Department of Material Science and Engineering, Massachusetts Institute of Technology, 77 Massachusetts Avenue, Cambridge, Massachusetts 02139-4307, USA*
(Received 30 July 2007; published 11 January 2008)

In the present contribution, we investigate how the electronic structure of a Au(111) surface covered by a self-assembled monolayer (SAM) of conjugated molecules depends on the packing density of the SAM. To that aim, biphenylthiol-based molecules bearing electron-rich and electron-poor substituents are studied by means of slab-type band-structure calculations. We find that the screening effects arising from the presence of neighboring molecules decisively influence the impact of the substituent as well as the adsorption-induced charge rearrangements at the metal-molecule interface. This has profound consequences not only for the alignment of the molecular levels with the Fermi energy and the SAM-induced work-function modification but also contributes to the clarification of the nature of the thiol-gold bond. The presented findings have important implications for single-molecule transport, SAM-based chemical sensing, and electrode modification in organic electronics.

DOI: 10.1103/PhysRevB.77.045113 PACS number(s): 71.15.Mb, 68.43.−h, 31.10.+z, 73.40.−c

I. INTRODUCTION

Self-assembled monolayers (SAMs) are widely used to modify and tune the physical properties of surfaces. Corrosion protection or change of wetting properties[1,2] can be achieved as well as modification of the substrate work function[3–6] and chemical sensing.[7,8] For the realization of organic electronic devices, the most important parameters are the work-function modification ($\Delta\phi$) and the alignment of the frontier molecular orbitals (MOs) with respect to the electrode Fermi level (E_F). While the former determines Schottky barrier heights,[9–13] which govern charge injection into organic devices, the latter is intrinsically connected with the electron-transport characteristics of single-molecule and monolayer devices.[14–20]

Recently, we reported on the interfacial processes governing these parameters for a variety of SAMs consisting of conjugated (semiconducting) molecules adsorbed onto metallic substrates.[21–23] The link between the alignment of the MOs and $\Delta\phi$ was established through the formation of dipole layers: one originates from the intrinsic dipole of the molecules realized by donor or acceptor substitution at the end of the backbone that is pointing away from the metal. A second dipole layer, the bond dipole, is due to the formation of the chemical bond between the docking group and the metal. It is largely independent of the substituent[22,24] but can be controlled through the choice of the docking group.[23]

In contrast to the previous investigations which were carried out for densely packed monolayers, here, in order to gain a deeper and more general insight, we systematically decrease the coverage θ of a SAM of 4′-substituted 4-mercaptobiphenyls adsorbed onto a Au(111) surface. We find a pronounced nonlinear coverage dependence of both $\Delta\phi$ and the alignment of the frontier MOs with E_F. These results are of special relevance for the entire field of single-molecule electronics, where vastly different coverages are probed depending on the experimental setup; more or less isolated molecules sandwiched between two electrodes are, for example, encountered in scanning tunneling spectroscopy measurements[25] of diluted monolayers or break-junction investigations,[26] while transport through more densely packed systems is studied in crossed-wire[27] or nanopore[28] experiments and large area[29] devices. Also in theoretical investigations, some studies use small metal clusters[30] as model for the electrodes (thus describing a single, isolated organic molecule), while calculations describing infinitely extended surfaces through periodic boundary conditions model the case of densely packed monolayers.[15–20]

The present contribution shows that varying the packing density of SAMs can lead to significantly altered electronic properties of one and the same type of molecule attached to the surface. In this context, it should be noted that the packing dependent mutual depolarization of adjacent molecules in one-dimensional and two-dimensional molecular clusters has recently been described using semiempirical techniques,[31] and Natan *et al.*[24] stressed the importance of cooperative effects (and the resulting molecular depolarization) at semiconductor/SAM interfaces.

Here, we also elucidate the nature of the thiol-gold interaction in terms of bonding-induced charge rearrangements at the metal-molecule interface, which lead to the formation of the bond dipole. This subject has been addressed in numerous experimental[5,6,10,32,33] and theoretical contributions[21–23,34–38] due to its relevance for $\Delta\phi$. In particular, we will show that, in the investigated systems, the adsorption-induced electron transfer from the molecular backbone to the sulfur (in the following denoted as R^+S^- following Ref. 6) is strongly pronounced at low coverages and suppressed in densely packed monolayers.

II. STRUCTURE OF THE SYSTEM

In this contribution, we employ the repeated slab approach, where the interface is modeled by a 2D-periodic in-

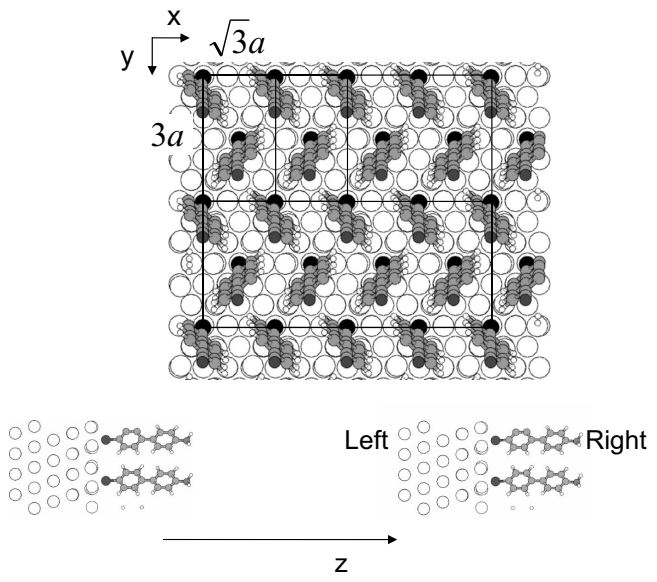

FIG. 1. Top: view of the biphenyl SAM adsorbed onto the Au(111) surface for $\theta=1$. The black squares represent the unit cells used to realize the lower coverages, as explained in the main text. Bottom: side view of the slabs used to describe the interface

finite sheet in the x-y plane (consisting of metal layers and the molecules), which is periodically repeated in the z direction. A vacuum gap of 22 Å is introduced between consecutive slabs to prevent interaction between them. The metal part of the slab is represented by five layers of gold. The slabs have two surfaces: the one to which the molecules are bonded is at larger z values and will be referred to as the right surface, and the other one will be denoted as the left surface (see Fig. 1). The vacuum regions next to the surfaces will be called the right and left vacuum regions accordingly.

The system under investigation consists of a SAM of 4′-substituted 4-mercaptobiphenyls assembled on Au(111). The unsubstituted SAM is known to pack in a dense herringbone pattern[39] and in this phase the system has previously been investigated by means of density-functional theory (DFT) calculations.[22] A top view of the Au(111) surface covered with the densely packed SAM is shown in Fig. 1. Two substitutions at the 4′-position are considered: an electron-poor cyano (-CN) group (acceptor) and an electron-rich amino ($-NH_2$) group (donor). They point away from the surface and provide the molecules with dipole moments pointing in opposite directions; these dipole moments will in the following be referred to as the *intrinsic* dipole moments. Additionally, the substituents significantly impact the ionization potentials of the isolated molecules.[22]

In most experimental setups, the actual microscopic interface and SAM structure can vary greatly. In certain break junctions, one is actually dealing with isolated molecules surrounded by solvent attached to a metal tip; in dilute monolayers, conjugated molecules are typically surrounded by alkane thiols, and in less densely packed and disordered SAMs, one can expect strong local fluctuations of the molecular orientation. Moreover, the existence of different structural phases in SAMs at different packing densities has been reported. For example, for 4′-methyl substituted 4-mercaptobiphenyl, a phase with the molecular backbones standing upright and one with the molecules virtually lying down on the surface has been observed in Ref. 40. While the many different possible geometric configurations can be expected to impact the interfacial electronic structure in the SAMs, a study of all possible cases encountered in experiments would obscure the more fundamental effects of coverage we seek to highlight in the present conceptual study.

Therefore, we chose to identify the purely electronic and electrostatic effects of a varying packing density by focusing on the most straightforward model case: we created submonolayers by consecutively removing molecules from the system optimized for full coverage ($\theta=1$), retaining an ordered superstructure. Half coverage ($\theta=1/2$) is achieved by removing one molecule out of the $\sqrt{3}\times 3$ surface unit cell (Fig. 1). Lower coverages are obtained by consecutively doubling the size of the unit cell and removing all molecules but one. In this way, $\theta=1/4$ and $\theta=1/8$ are realized through $2\sqrt{3}\times 3$ and $4\sqrt{3}\times 3$ surface unit cells. $\theta=1/16$ is obtained by doubling the unit-cell size at $\theta=1/8$ along the y direction. Although this does not provide a one-to-one correspondence to any one particular experimental situation, we are confident that the gained fundamental insight justifies our approach, as it provides general guidelines for the understanding of coverage-related effects in the interfacial electronic structure of SAMs on metals.

In order to clearly discriminate between effects arising from intermolecular interactions and effects due to the bonding of the molecule to the metal, calculations were carried out separately for the organic layer alone and for the monolayer adsorbed onto the substrate. In order to always deal with saturated docking groups, the sulfur moieties are saturated with hydrogen atoms in the case of the isolated monolayer. The position of the hydrogen atom is determined by a geometry optimization where only the hydrogen atom is allowed to relax, while the monolayer itself is kept in the geometry it adopts when bonded to the metal. For calculating the properties of an isolated molecule, it is placed in a very large unit cell corresponding to a coverage of $\theta=1/64$. This is realized by doubling the unit cell at $\theta=1/16$ in the x and y directions omitting the metal.

For all coverages, the molecules are initially kept frozen at the equilibrium geometry at full coverage[22] to highlight effects which are of purely electronic nature. Geometric relaxations together with their consequences are then discussed briefly in the Appendix for $\theta=1/2$ and $\theta=1/4$. For lower coverages and the corresponding huge surface unit cells, geometry optimizations are computationally too demanding.

III. COMPUTATIONAL METHODOLOGY

DFT calculations with the PW91 exchange-correlation functional were performed with a plane-wave basis set (cutoff of 20 Ry) using the VASP code.[41–44] The projector augmented-wave method[45,46] was applied to describe valence-core interactions. This allows for the relatively low kinetic energy cutoff for the plane-wave basis set. $8\times 5\times 1$, $8\times 5\times 1$, $4\times 5\times 1$, $2\times 5\times 1$, $2\times 2\times 1$, and $1\times 1\times 1$ Monkhorst-Pack grids[47] of k points were applied for cover-

ages of $\theta=1$, 1/2, 1/4, 1/8, 1/16, and 1/64, respectively. This ensures consistent k point sampling for all unit-cell sizes; moreover, a Methfessel-Paxton occupation scheme (broadening 0.2 eV) was used.[48]

Following the approach outlined in Refs. 21–23, the energetic position of the states derived from the highest occupied MO (HOMO) of the isolated molecule relative to E_F was determined by the first pronounced peak (below E_F) of the purely molecular contribution to the total density of states of the metal/SAM system.

For practical reasons, a dipole sheet is introduced in the middle of the vacuum gap between two consecutive slabs.[49] This procedure allows extracting the work functions of the asymmetric slabs on the right and left sides by evaluating the difference between the Fermi energy of the system and the value of the local electrostatic potential in the vacuum region on the respective side of the slab.

Geometry optimizations were carried out using a damped molecular dynamics scheme until the remaining forces were <0.01 eV/Å. The three bottom metal layers of the five-layer slab were always kept fixed at their bulk geometry; the sulfur docking atom is found to be situated in the fcc hollow with only a minor distortion toward the bridge site. Three-dimensional graphics were produced using XCRYSDEN.[50]

IV. RESULTS AND DISCUSSION

To distinguish between effects arising from the interaction of the molecules within the monolayer and between the monolayer and the metal substrate, we first considered the electronic structures of the noninteracting metal and SAM systems. The combined system will be treated in the subsequent sections dealing with the results of bond formation and the resulting charge redistributions.

A. Isolated self-assembled monolayer

When arranging molecules with an intrinsic dipole moment in a regular fashion in the x-y plane, a dipole layer is formed. The area density of molecules is given by θ/A, where $A=22.6$ Å^2 is half of the area of the $\sqrt{3}\times 3$ unit cell in the x-y plane. The potential energy of an electron E_e (defined as the energy of a particle with negative elementary charge) in such a monolayer (as obtained from the DFT calculation) can be visualized along the z axis by averaging over all points in the x-y plane. In Fig. 2, E_e is shown for the -NH_2 substituent at $\theta=1$ (solid line). One conceptually important feature is that E_e assumes two distinct values, E_{vac}^{left} and E_{vac}^{right}, on the left and right sides of the monolayer. The difference $\Delta E_{vac}=E_{vac}^{right}-E_{vac}^{left}$ is directly related to the molecular dipole moment and the area density of molecules in the SAM through the Helmholtz equation

$$\Delta E_{vac}(\theta)=\frac{e\theta\mu(\theta)}{A\varepsilon_0}. \quad (1)$$

Here, $\mu(\theta)$ is the component of the molecular dipole moment in the z direction.

At $\theta=1/16$, the plane averaged potential energy of an electron has a somewhat different shape, as shown by the dashed-dotted line in Fig. 2 (V_e at $\theta=1/16$ has been multiplied by a factor of 16 and the E_{vac}^{right} have been aligned). In contrast to E_e for $\theta=1$, a gradual decrease of the averaged energy from left to right can be seen, which is a consequence of the presence of an electric field within the monolayer. For larger coverages, this field is increasingly screened by the neighboring molecules resulting in a reduced net dipole moment per molecule.[7,31,51–53] It should also be mentioned that in a purely classical model viewing the substituents as mere point dipoles, the field penetration is also reduced for small dipole-dipole distances.[24]

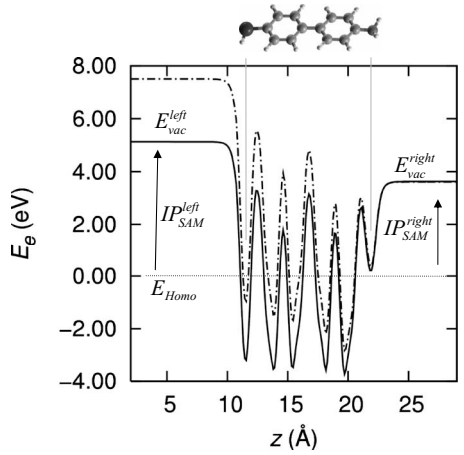

FIG. 2. Potential energy of an electron E_e in the -NH_2 substituted monolayer at $\theta=1$ (solid line) and $\theta=1/16$ (dashed-dotted line). To allow for better comparison, the latter curve was multiplied by a factor of 16 and the E_{vac}^{right} were aligned.

As a consequence of this depolarization, μ is significantly reduced upon increasing θ, which gives rise to the markedly sublinear coverage dependence of ΔE_{vac} (shown for both substituents in the top part of Fig. 3). The limiting case of no intermolecular interactions is given by setting $\mu(\theta)=\mu^0$ in Eq. (1), with μ^0 being the z component of the intrinsic dipole moment of the isolated molecules ($\mu^0=-0.51$ e Å$=-2.45$ D and $\mu^0=1.14$ e Å$=5.48$ D for the -NH_2 and -CN substitutions, respectively). The resulting linear dependence of ΔE_{vac} on θ is indicated by the solid lines in Fig. 3 (top). The marked differences between the evolutions with and without considering the intermolecular interactions highlights the importance of coverage effects, especially for high packing densities.

When neglecting effects due to the interaction between metal and SAM (i.e., for the case discussed in the present section), ΔE_{vac} equals the work-function modification $\Delta\phi$ of the SAM covered Au(111) surface relative to the pristine Au surface. This is the relevant quantity for many applications of SAMs in organic electronics that aim at tuning charge injection barriers at interfaces. The data in Fig. 3 also underline that introducing a (coverage-independent) "effective" dielectric constant into the denominator of Eq. (1)[3–5,10] is not sufficient. This would only change the slopes of the solid lines in Fig. 3 but fail to capture the pronounced nonlinearity of $\Delta E_{vac}(\theta)$.

To discuss the relative alignment of metal and molecular states, the next quantity to be addressed is the ionization

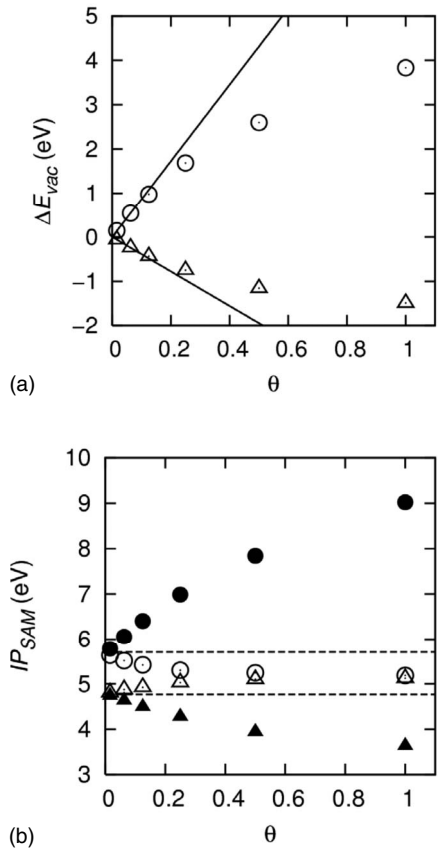

FIG. 3. Top: potential energy jump ΔE_{vac} as a function of coverage θ as calculated by DFT (symbols) and from the Helmholz equation (solid lines). Triangles (circles) refer to the -NH_2 (-CN) substitution. Bottom: IP^{left}_{SAM} (open symbols) and IP^{right}_{SAM} (filled symbols) for the -NH_2 (triangles) and -CN (circles) substituents as a function of θ. The dashed lines represent the IPs of the isolated molecules.

potential of the isolated monolayer. In the bottom part of Fig. 3, we show the evolution of the ionization potentials (IPs) of the SAMs with θ. For the isolated molecules, there exists only one IP, which is in a first approximation given by the energetic position of the HOMO relative to one unique vacuum level. It is calculated to be 4.78 eV for the electron-rich -NH_2 substituent and 5.60 eV for the electron-poor -CN substituent. In contrast, for the SAM, there are two distinct IPs, IP^{left}_{SAM} and IP^{right}_{SAM}, as there are two distinct vacuum levels E^{left}_{vac} and E^{right}_{vac} split by ΔE_{vac} (see above and Fig. 2). For $\theta=0$, ΔE_{vac} vanishes and $IP^{left}_{SAM}=IP^{right}_{SAM}=IP$; upon increasing θ, IP^{left}_{SAM} and IP^{right}_{SAM} start deviating from the respective IP value with the largest differences for $\theta=1$. In that case, IP^{left}_{SAM} is completely insensitive to the substituent.[22]

IP^{left}_{SAM} is a crucial quantity for the alignment of the frontier molecular orbitals with respect to the Fermi level: in the (hypothetical) case of no electronic interaction between metal and SAM, i.e., in the Schottky-Mott limit, the left vacuum level E^{left}_{vac} of the isolated monolayer aligns with the vacuum level above the Au(111) surface. Then, the position of the HOMO relative to the Fermi level is simply given by $\Delta E^{n.i.}_{HOMO}=\phi_{Au(111)}-IP^{left}_{SAM}$. $\phi_{Au(111)}$ is the work function of the Au(111) surface and was calculated to be 5.2 eV.[21] Following the evolution of IP^{left}_{SAM}, $\Delta E^{n.i.}_{HOMO}$ at $\theta=1$ is independent of the substitution and the molecular HOMO is located close to the Fermi level (see Fig. 4, open symbols). At lower θ values, the -NH_2 (-CN) substituted monolayer has the HOMO located well above (below) the Fermi level with the biggest differences between the two systems observed for θ approaching 0, i.e., for the limit of quasi-isolated molecules.

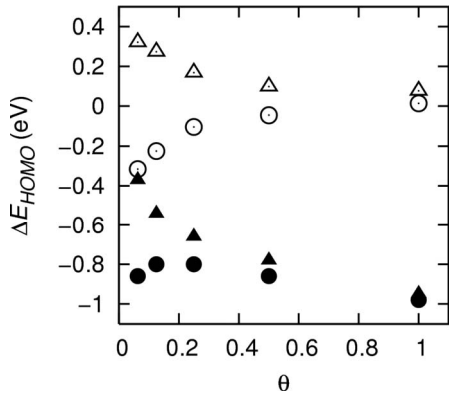

FIG. 4. HOMO energies with respect to the Fermi level in the noninteracting case, $\Delta E^{n.i.}_{HOMO}$ (open symbols), and in the interacting case, ΔE_{HOMO} (filled), as a function of coverage θ. Triangles (circles) refer to the -NH_2 (-CN) substitution.

B. Charge rearrangements upon bond formation

When allowing SAM and metal to interact and to form a chemical bond, rearrangements in the charge density, $\Delta\rho_{bond}$, occur at the interface. To calculate $\Delta\rho_{bond}$, the noninteracting electron density is subtracted from the electron density ρ of the combined metal-monolayer system.[21–23] The former is derived from the electron density of the isolated metal slab, $\rho_{Au(111)}$, the isolated monolayer, ρ_{mono}, and the isolated hydrogen atoms, ρ_H. For the z-dependent quantities per molecule one obtains by integration over the xy plane within the unit cell,

$$\Delta\rho_{bond}(z)=\frac{1}{M}\{\rho(z)-[\rho_{Au(111)}(z)+\rho_{mono}(z)-\rho_H(z)]\}. \quad (2)$$

Here, M denotes the number of molecules in the unit cell.

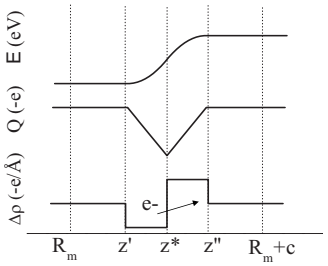

FIG. 5. Charge rearrangements $\Delta\rho_{bond}$ (bottom), amount of transferred charge Q_{bond} (center), and resulting potential energy of an electron E_{bond} (top) for an idealized simple electron transfer case, where an electron is removed from the region between z' and z^* and placed in the region between z^* and z''. R_m denotes the middle of the vacuum gap and c is the unit-cell vector along the z direction.

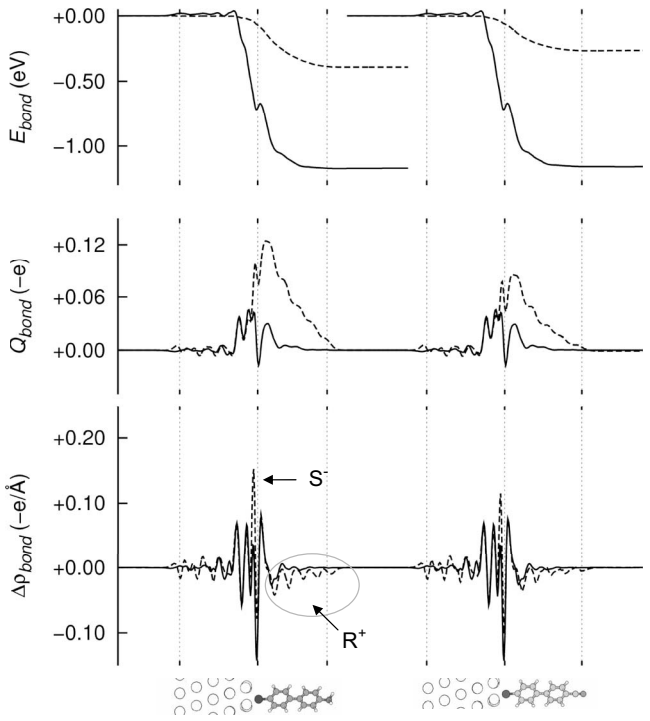

FIG. 6. Charge rearrangement $\Delta\rho_{bond}$ and charge transfer Q_{bond} (definition see text) per molecule as well as the resulting potential energy of an electron, E_{bond} for the -NH_2 (left) and -CN (right) substituted monolayers. $\Delta\rho_{bond}$ and Q_{bond} have been integrated over the x-y plane of the respective surface unit cell. The solid lines correspond to $\theta=1$ and the dashed lines to $\theta=1/16$.

In order to facilitate the interpretation of $\Delta\rho_{bond}$, we first consider a simplified one-dimensional case where a dipole layer is created through transfer of one electron from the region between $-z'$ and z^* to the region between z^* and z''. $\Delta\rho_{bond}(z)$ is then given by step functions, as shown in Fig. 5. In order to quantify the amount of charge transfer occurring upon adsorption, one can consider Q_{bond}, which is calculated by integrating $\Delta\rho_{bond}$ over z,

$$Q_{bond}(z) = \int_{-\infty}^{z} \Delta\rho_{bond}(z')dz'. \tag{3}$$

In the example in Fig. 5, Q_{bond} adopts a triangular shape with $Q_{bond}(z^*)=e$, i.e., the maximum of Q_{bond} equals the total amount of transferred charge. The corresponding potential energy of an electron, $E_{bond}(z)$, is then obtained by solving the one-dimensional Poisson equation (e being the elementary charge; see also Fig. 5),

$$\frac{d^2E_{bond}(z)}{dz^2} = \frac{e\theta}{\varepsilon_0 A}\Delta\rho_{bond}(z). \tag{4}$$

For the case of the biphenyl-type SAMs adsorbed on Au(111), $\Delta\rho_{bond}$ and its impact on level alignment and work-function modification have already been discussed for full coverage ($\theta=1$).[22] Here, we will focus on differences arising from variations in the packing density. In Fig. 6, $\Delta\rho_{bond}$ at $\theta=1$ and $\theta=1/16$ are compared. All intermediate densities (not shown) lie between these two limiting cases.

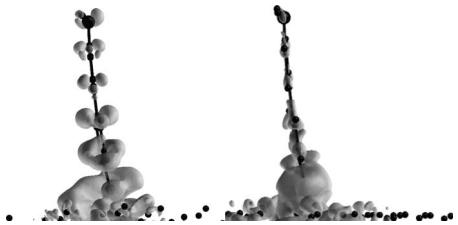

FIG. 7. Isodensity representation of $\Delta\rho_{bond}(x,y,z)$ at $\theta=1/16$ for the -NH_2 substituent. The molecule is shown from the side, i.e., the plane of the biphenyl backbone is vertical to the drawing plane to show the π character of the electron depletion in the backbone. Electrons flow from the regions shown in the left image to the regions shown in the right image.

To analyze local charge redistributions, we will focus on $\Delta\rho_{bond}$, while the net charge transfer between larger regions is best revealed by close to triangular features in Q_{bond} (see above). At high coverage, we see in the molecular region (encircled in Fig. 6) that the rapidly varying features of $\Delta\rho_{bond}$ are of positive and negative signs and decay rapidly at larger distances from the immediate metal-molecule interface. The small triangular feature of Q_{bond} in the region between the sulfur atom and the first three carbon atoms is indicative of electron density being shifted toward the sulfur region. In the region of the metal, $\Delta\rho_{bond}$ displays much larger oscillations. The feature seen for Q_{bond} between the second metal layer and the sulfur atom is a clear indication of electron density being shifted from the interface region to the first approximately. 1.5 layers of gold. This feature is attributed to the bond formation between sulfur and gold and the *push-back* effect arising from Pauli repulsion, i.e., the electron density leaking out from the pristine metal surface into the vacuum is pushed back into the metal due to the mere presence of the molecules.[54] The fact that the two close to triangular features of Q_{bond} are relatively well separated by a minimum at the position of the S atom with $Q_{bond}\approx 0$ shows that there is virtually no net charge transfer between the metal and the molecules.

At low θ, the features of $\Delta\rho_{bond}$ in the molecular region are all of negative sign and decay much more gradually over the molecule. Here, the depletion of electrons from the backbone (R^+) is accompanied by a sharply localized accumulation of electrons in the sulfur and interface region (S^-) which justifies the term R^+-S^- electron transfer previously used for thiol-bonded SAMs.[6] Within the metal, the main difference between high and low coverages is that in the latter case, the charge redistributions are no longer confined to the two topmost layers but extend over the whole five-layer slab (see Fig. 6). The lack of strong features in Q_{bond} in the region of the three bottom layers, however, shows that these fluctuations are of only local nature and are not associated with long-range charge transfer.

Furthermore, while at high coverage there is virtually no difference between the -NH_2 and -CN substituted SAMs, the R^+-S^- electron transfer at low coverage is much more pronounced for the -NH_2 substituent. This can be explained by the fact that -NH_2 as a donor promotes the transfer in contrast to -CN, which as an acceptor counteracts it.

The spatial distribution of $\Delta\rho_{bond}$ at low coverage is visualized by an isodensity representation in Fig. 7. It shows that

the electron transfer from the backbone to the interface (sulfur) region occurs from the π system of the molecule. In contrast to the previous analysis for high coverage at $\theta=1$,[21] here, the entire backbone is involved in the process consistent with electron transfer being much more pronounced at low coverage.

$E_{bond}(z)$ as induced by the charge rearrangements [see Fig. 6 and Eq. (4)] displays a steplike shape of magnitude BD(θ). It is smaller at low coverage despite the fact that then the electron transfer per molecule is more pronounced. This follows from the linear scaling of E_{bond} with the packing density θ [Eq. (4)]. The bond dipole moment μ_{bond}, however, which is again defined per molecule as

$$\mu_{bond} = \frac{A\varepsilon_0}{\theta e}\mathrm{BD}(\theta), \tag{5}$$

is much more pronounced at low coverage. At $\theta=1$, $\mu_{bond}=-0.15\ e$ Å (−0.72 D) for both the -NH_2 and -CN cases, while for $\theta=1/16$, $\mu_{bond}=-0.79\ e$ Å (−3.79 D) for the -NH_2 and $\mu_{bond}=-0.54\ e$ Å (−2.59 D) for the -CN substituents. This shows that the dipole is not only substantially bigger at low coverage but also highly sensitive to the substituent, i.e., the chemical structure of the SAM.

C. Implication of the charge rearrangements for work-function changes and level alignment

This is of relevance for previous works,[3–5,10] where the SAM-induced work-function modifications are estimated based on the intrinsic dipole moments of the molecules, μ, and a certain bond dipole μ_{bond}. Our findings, however, underline that both dipoles are highly depending on coverage; μ because of the screening of the molecular dipole moments by the neighboring molecules and the resulting depolarization and μ_{bond} as a consequence of the coverage dependent R^+-S^- transfer. The localization of this charge transfer at high coverage can again be attributed to the screening properties of the neighboring biphenyl backbones, effectively decoupling the sulfur end of the monolayer from the substituent end. We believe this screening effect to be of relevance also for chemical sensing based on the cooperative molecular field effect,[7] where chemical substitution on one side of the molecular layer induces a charge redistribution on the other end. According to the present findings, the redistributions per molecule will be strongly suppressed at high coverage.

In general, the total coverage-dependent work-function modification $\Delta\phi(\theta)$ is obtained via[21–23]

$$\Delta\phi(\theta) = \mathrm{BD}(\theta) + \Delta E_{vac}(\theta). \tag{6}$$

It is shown as a function of θ in Fig. 8. For comparative reasons, the solid lines from Fig. 2, which depict the situation neglecting depolarization and the bond dipole, are included as well. A comparison of Figs. 2 and 8 reveals that, due to BD(θ), $\Delta\phi(\theta)$ is systematically shifted to more negative values compared to $\Delta E_{vac}(\theta)$. Interestingly, in contrast to what was observed for $\Delta E_{vac}(\theta)$, an almost linear increase of $\Delta\phi$ is now obtained for the -CN substituent, although the slope is much smaller than one would expect when only considering the intrinsic molecular dipole moment (compare the straight line in Fig. 8). For the -NH_2 substituent, a clearly sublinear evolution is observed. The significant differences in the θ dependence of $\Delta\phi(\theta)$ between the two substitutents are due to the fact that $\Delta V_{vac}(\theta)$ and BD(θ), which add up for the -NH_2 substituent but partly cancel for -CN, display somewhat different evolutions with θ. Moreover, these evolutions are not the same for the two investigated systems. This shows that if one intends to modify, e.g., the work function of electrodes by adsorbing chemically bonded SAMs, changes in the chemical structure of the molecule can have profound effects for the dependence of the work-function modification on the film quality (exemplified here by the packing density).

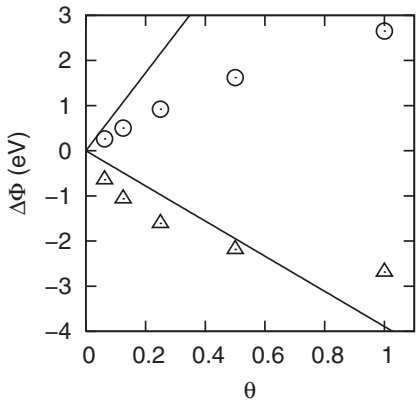

FIG. 8. Work-function modification $\Delta\phi(\theta)$ induced by the SAM in the combined metal-molecule system as a function of coverage θ. Open symbols refer to the calculations where the geometries were kept fixed to the equilibrium geometry at $\theta=1$. Triangles (circles) refer to the -NH_2 (-CN) substitution.

In Fig. 4, we show how the HOMO-derived state in the combined metal-molecule system aligns relative to the Fermi level. The energy difference ΔE_{HOMO} between this state and E_F is a direct measure for the hole-injection barrier from the metal into the SAM. The HOMO is systematically downshifted compared to the noninteracting case discussed in Sec. IV A (ΔE_{HOMO} is clearly more negative than $\Delta E^{n.i.}_{HOMO}$ in Fig. 4). This is a direct consequence of E_{bond}, which shifts the potential landscape in the molecular region to lower energies. As a result, when including the bond dipole, the HOMO is located clearly *below* the Fermi level of the metal in all investigated cases.

A closer analysis of the trends reveals that, in fact, ΔE_{HOMO} cannot be directly obtained by simply adding BD to the HOMO position in the noninteracting case. Rather, a small correction term $E_{corr}(\theta)$ has to be added,[23] which turns out to be also coverage dependent, as shown in Fig. 9,

$$\Delta E_{HOMO}(\theta) = \Delta E^{n.i.}_{HOMO} + \mathrm{BD}(\theta) + E_{corr}(\theta). \tag{7}$$

We assign the origin of $E_{corr}(\theta)$ to two competing contributions. (i) The potential drop BD is not sudden at the interface (Fig. 6); thus, the potential well of the molecule is perturbed close to the interface resulting in an upward shift of the HOMO. (ii) The π-conjugated backbone of the molecule is

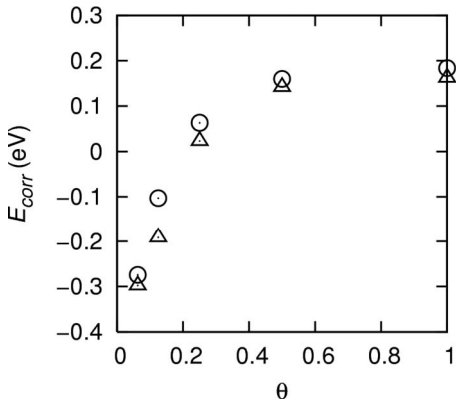

FIG. 9. Energy correction of the molecular states, E_{corr}, resulting from the change of the molecular potential as a function of coverage θ. Triangles (circles) refer to the -NH_2 (-CN) substitution.

depleted of electrons due to R^+-S^- charge transfer and the resulting unscreening of the nuclei introduces a downshift of the HOMO. As the latter effect gains in importance upon lowering the coverage, we see a transition from positive $E_{corr}(\theta)$ at high θ toward negative $E_{corr}(\theta)$ at low θ.

Importantly, Fig. 4 clearly shows that there still exists a strong correlation between $\Delta E^{n.i.}_{HOMO}(\theta)$ and $\Delta E_{HOMO}(\theta)$. In particular, the negligible difference between the two substituents at $\theta=1$ and the significant difference at $\theta=1/16$ is preserved. This underlines that for tuning the level alignment of molecules on surfaces, the control of IP^{left}_{SAM} is of great importance.[23] Most importantly, for single-molecule transport applications, the observation of a highly coverage-dependent level alignment implies that the *I-V* characteristics of a single isolated molecule between two contacts can be markedly different from those of a densely packed monolayer of the same molecule.

V. SUMMARY AND CONCLUSIONS

We investigated the coverage dependence of the electronic structure of biphenylthiol-based SAMs on the Au(111) surface. Two different substituents, an electron-rich -NH_2 and an electron-poor -CN group, were attached to the top end of the molecules to provide them with different molecular ionization potentials and to realize SAMs with opposite dipole moments.

For the isolated monolayers (no metal present), we observed energetic decoupling of the substituent side from the thiol side (found in Ref. 22) only at high coverage, where effects due to end-group substitution are efficiently screened by the polarizable π-conjugate backbone of the molecules. These screening effects result in a (nonlinear) reduction of the dipole moments of the molecules with increasing packing densities (depolarization). At low coverage, an electric field arising from the intrinsic dipole moments of the SAM forming molecules is present in the loosely packed layer.

For the interacting SAM/Au(111) system, a markedly coverage-dependent electron transfer from the entire conjugated backbone toward the sulfur and interface region is observed (R^+-S^- charge transfer) at low packing densities. It is more pronounced for the -NH_2 than for the -CN substituent. At high coverage, the electronic rearrangements upon Au—S bond formation are confined largely to the sulfur region and, consequently, are unaffected by the substituent.

The SAM-induced work-function modification (originating from the molecular dipoles and the Au—S bond dipole) also displays a pronounced coverage dependence. Interestingly, the observed trends differ significantly for the two substituents. While in the -CN case the work-function modification is seen to depend almost linearly on the coverage, it is strongly sublinear for the -NH_2 substituent. This is highly relevant for the more and more common application of SAMs for tuning the charge injection properties of electrodes in organic electronics.

Additionally, the packing density of the molecules in the SAM has a profound impact on the energetic alignment between the frontier molecular orbitals and the metal Fermi level. Therefore, the electron-transport characteristics of single-molecular junctions can be expected to be strongly influenced by the presence of neighboring molecules and the corresponding packing density. We conclude that, for an efficient design of SAM-based molecular electronics, coverage-related effects do play a decisive role.

ACKNOWLEDGMENTS

The authors would like to acknowledge the financial support by the Austrian Science Foundation (FWF) through the Austrian Nano Initiative (Project No. N-702-SENSPHYS) and by the European Community project "IControl" (EC-STREP-033197). G.H. is supported by the INSANE project (Marie Curie, OIF Contract No. 021511). The authors are also grateful to Robert Schennach for stimulating discussions and to the section "Computing & Application Services" of the Zentrale Informatikdienst of the Graz University of Technology as well as to the group of J. L. Brédas for providing computational resources and to the Institut für Materialphysik of the Universität Wien for providing the VASP code.

APPENDIX: GEOMETRY RELAXATIONS

For the higher packing densities, steric hindrance amongst the molecules constrains their atomic structure. When performing a structural relaxation of a completely isolated molecule (no surface included), two major differences are observed with respect to the geometries considered so far: (i) the inter-ring twist angle between the two central phenyl rings is increased from 5.6° to 24.6°, which results in an increase of the band gap by 0.2 eV, and (ii) some bond lengths are modified. In particular, the bond length from the outer phenylene to the substituent changes from 1.415 to 1.399 Å in the -NH_2 case, while it remains largely constant for the -CN substituent (1.427 and 1.428 Å). Due to this distortion, the intrinsic dipole moment of the -NH_2 substituted molecule increases from −0.51 *e Å* (−2.45 D) to −0.58 *e Å* (−2.79 D), while in the -CN case it remains at 1.14 *e* Å. (2.48 D). The difference between -NH_2 and -CN can be rationalized by the fact that for -NH_2, two different resonance structures exist, R—NH_2 and R^-=NH_2^+, which

is empirically known to result in the observed bond-length changes. Such two resonance structures are not possible for the -CN substituent.

The situation of relaxing the molecules on the surface is very similar to the case just described. These relaxations were investigated for the $\theta=1/2$ and $\theta=1/4$ systems and were started from the geometries considered before. The inclination of the long molecular axis with respect to the surface normal was not changed during the optimization, while the molecule approaches the surface by about 0.2 Å at $\theta=1/4$. The latter is consistent with the before-mentioned increase of electron density in the spatial region between sulfur and gold. For $\theta=1/4$, the inter-ring twist angle increases to 23° which is very close to the value of the isolated molecule. This can be rationalized in terms of the intermolecular packing forces being already largely reduced at this coverage.

The fact that the molecules approach the surface slightly increases BD and, as a consequence, also the energy levels of the molecule are slightly lowered (~0.1 eV) in agreement with Ref. 55, where the effect of increasing the distance to the surface was studied in detail for dithiolbenzene. The relaxations make the previously discussed differences in the coverage dependence of $\Delta\phi(\theta)$ even more pronounced. Now, in the $-NH_2$ substituted monolayer, $|\Delta\phi|$ increases by only 8% (instead of 23%) when going from half coverage to full coverage, whereas a 73% (instead of a 63%) increase is observed for the -CN substituted monolayer.

[1] J. Genzer and K. Efimenko, Science **290**, 2130 (2000).
[2] G. K. Jennings and P. E. Laibinis, Colloids Surf., A **116**, 105 (1996).
[3] B. de Boer, A. Hadipour, M. M. Mandoc, T. van Woudenbergh, and P. W. M. Blom, Adv. Mater. (Weinheim, Ger.) **17**, 621 (2005).
[4] R. W. Zehner, B. F. Parsons, R. P. Hsung, and L. R. Sita, Langmuir **15**, 1121 (1999).
[5] D. M. Alloway, M. Hofmann, D. L. Smith, N. E. Gruhn, A. L. Graham, R. Colorado, V. H. Wysocki, T. R. Lee, P. A. Lee, and N. R. Armstrong, J. Phys. Chem. B **107**, 11690 (2003).
[6] S. D. Evans and A. Ulman, Chem. Phys. Lett. **170**, 462 (1990).
[7] D. Cahen, R. Naaman, and Z. Vager, Adv. Funct. Mater. **15**, 1571 (2005).
[8] X. F. Guo, M. Myers, S. X. Xiao, M. Lefenfeld, R. Steiner, G. S. Tulevski, J. Y. Tang, J. Baumert, F. Leibfarth, J. T. Yardley, M. L. Steigerwald, P. Kim, and C. Nuckolls, Proc. Natl. Acad. Sci. U.S.A. **103**, 11452 (2006).
[9] I. H. Campbell, J. D. Kress, R. L. Martin, D. L. Smith, N. N. Barashkov, and J. P. Ferraris, Appl. Phys. Lett. **71**, 3528 (1997).
[10] I. H. Campbell, S. Rubin, T. A. Zawodzinski, J. D. Kress, R. L. Martin, D. L. Smith, N. N. Barashkov, and J. P. Ferraris, Phys. Rev. B **54**, R14321 (1996).
[11] C. Ganzorig, K. J. Kwak, K. Yagi, and M. Fujihira, Appl. Phys. Lett. **79**, 272 (2001).
[12] H. Yan, Q. L. Huang, J. Cui, J. G. C. Veinot, M. M. Kern, and T. J. Marks, Adv. Mater. (Weinheim, Ger.) **15**, 835 (2003).
[13] L. Zuppiroli, L. Si-Ahmed, K. Kamaras, F. Nuesch, M. N. Bussac, D. Ades, A. Siove, E. Moons, and M. Gratzel, Eur. Phys. J. B **11**, 505 (1999).
[14] S. Datta, *Electronic Transport in Mesoscopic Systems* (Cambridge University Press, Cambridge, 1995).
[15] A. Calzolari, N. Marzari, I. Souza, and M. B. Nardelli, Phys. Rev. B **69**, 035108 (2004).
[16] P. S. Damle, A. W. Ghosh, and S. Datta, Phys. Rev. B **64**, 201403 (2001).
[17] M. Di Ventra, S. T. Pantelides, and N. D. Lang, Phys. Rev. Lett. **84**, 979 (2000).
[18] J. Heurich, J. C. Cuevas, W. Wenzel, and G. Schon, Phys. Rev. Lett. **88**, 256803 (2002).
[19] J. J. Palacios, A. J. Pérez-Jiménez, E. Louis, and J. A. Vergés, Phys. Rev. B **64**, 115411 (2001).
[20] J. Taylor, H. Guo, and J. Wang, Phys. Rev. B **63**, 245407 (2001).
[21] G. Heimel, L. Romaner, J. L. Bredas, and E. Zojer, Surf. Sci. **600**, 4548 (2006).
[22] G. Heimel, L. Romaner, J. L. Bredas, and E. Zojer, Phys. Rev. Lett. **96**, 196806 (2006).
[23] G. Heimel, L. Romaner, E. Zojer, and J. L. Bredas, Nano Lett. **7**, 932 (2007).
[24] A. Natan, Y. Zidon, Y. Shapira, and L. Kronik, Phys. Rev. B **73**, 193310 (2006).
[25] M. T. Cygan, T. D. Dunbar, J. J. Arnold, L. A. Bumm, N. F. Shedlock, T. P. Burgin, L. Jones, D. L. Allara, J. M. Tour, and P. S. Weiss, J. Am. Chem. Soc. **120**, 2721 (1998).
[26] M. A. Reed, C. Zhou, C. J. Muller, T. P. Burgin, and J. M. Tour, Science **278**, 252 (1997).
[27] J. G. Kushmerick, J. Naciri, J. C. Yang, and R. Shashidhar, Nano Lett. **3**, 897 (2003).
[28] J. Chen, M. A. Reed, A. M. Rawlett, and J. M. Tour, Science **286**, 1550 (1999).
[29] H. B. Akkerman, P. W. M. Blom, D. M. de Leeuw, and B. de Boer, Nature (London) **441**, 69 (2006).
[30] H. B. Weber, J. Reichert, F. Weigend, R. Ochs, D. Beckmann, M. Mayor, R. Ahlrichs, and H. von Lohneysen, Chem. Phys. **281**, 113 (2002).
[31] D. Cornil, Y. Olivier, V. Geskin, and J. Cornil, Adv. Funct. Mater. **17**, 1143 (2007).
[32] S. Howell, D. Kuila, B. Kasibhatla, C. P. Kubiak, D. Janes, and R. Reifenberger, Langmuir **18**, 5120 (2002).
[33] F. Bussolotti, M. G. Betti, and C. Mariani, Phys. Rev. B **74**, 125422 (2006).
[34] J. A. Rodriguez, J. Dvorak, T. Jirsak, G. Liu, J. Hrbek, Y. Aray, and C. Gonzalez, J. Am. Chem. Soc. **125**, 276 (2003).
[35] V. De Renzi, R. Rousseau, D. Marchetto, R. Biagi, S. Scandolo, and U. del Pennino, Phys. Rev. Lett. **95**, 046804 (2005).
[36] H. Gronbeck, A. Curioni, and W. Andreoni, J. Am. Chem. Soc. **122**, 3839 (2000).
[37] M. Konopka, R. Rousseau, I. Stich, and D. Marx, J. Am. Chem. Soc. **126**, 12103 (2004).
[38] A. Bilic, J. R. Reimers, and N. S. Hush, J. Chem. Phys. **122**, 094708 (2005).
[39] F. Schreiber, Prog. Surf. Sci. **65**, 151 (2000).

[40] T. Y. B. Leung, P. Schwartz, G. Scoles, F. Schreiber, and A. Ulman, Surf. Sci. **458**, 34 (2000).
[41] G. Kresse and J. Furthmuller, Comput. Mater. Sci. **6**, 15 (1996).
[42] G. Kresse and J. Hafner, Phys. Rev. B **47**, 558 (1993).
[43] G. Kresse and J. Hafner, Phys. Rev. B **49**, 14251 (1994).
[44] G. Kresse and J. Furthmüller, Phys. Rev. B **54**, 11169 (1996).
[45] P. E. Blöchl, Phys. Rev. B **50**, 17953 (1994).
[46] G. Kresse and D. Joubert, Phys. Rev. B **59**, 1758 (1999).
[47] H. J. Monkhorst and J. D. Pack, Phys. Rev. B **13**, 5188 (1976).
[48] M. Methfessel and A. T. Paxton, Phys. Rev. B **40**, 3616 (1989).
[49] J. Neugebauer and M. Scheffler, Phys. Rev. B **46**, 16067 (1992).
[50] A. Kokalj, Comput. Mater. Sci. **28**, 155 (2003).
[51] D. M. Taylor and G. F. Bayes, Phys. Rev. E **49**, 1439 (1994).
[52] B. L. Maschhoff and J. P. Cowin, J. Chem. Phys. **101**, 8138 (1994).
[53] J. Topping, Proc. R. Soc. London, Ser. A **114**, 67 (1927).
[54] G. Witte, S. Lukas, P. S. Bagus, and C. Woll, Appl. Phys. Lett. **87**, 263502 (2005).
[55] L. Romaner, G. Heimel, M. Gruber, J. L. Bredas, and E. Zojer, Small **2**, 1468 (2006).